Investigating the Influence of Flip Angle and *k*-Space Sampling on Dynamic Contrast-Enhanced MRI Breast Examinations

Araminta E. W. Ledger, PhD, Marco Borri, MPhys, Romney J. E. Pope, MRCP, FRCR, Erica D. Scurr, BSc, Toni Wallace, BSc, Cheryl Richardson, DCR(R), Marianne Usher, MSc, Steven Allen, MRCS, FRCR, Robin M. Wilson, FRCR, FRCPE, Karen Thomas, PhD, Nandita M. deSouza, MD, FRCR, Martin O. Leach, PhD, FMedSci, Maria A. Schmidt, PhD

Rationale and Objectives: To retrospectively investigate the effect of flip angle (FA) and *k*-space sampling on the performance of dynamic contrast-enhanced (DCE-) magnetic resonance imaging (MRI) breast sequences.

Materials and Methods: Five DCE-MRI breast sequences were evaluated (10°, 14°, and 18° FAs; radial or linear *k*-space sampling), with 7–10 patients in each group ($n = 45$). All sequences were compliant with current technical breast screening guidelines. Contrast agent (CA) uptake curves were constructed from the right mammary artery for each examination. Maximum relative enhancement, E_{max}, and time-to-peak enhancement, T_{max}, were measured and compared between protocols (analysis of variance and Mann–Whitney). For each sequence, calculated values of maximum relative enhancement, E_{calc}, were derived from the Bloch equations and compared to E_{max}. Fat suppression performance (residual bright fat and chemical shift artifact) was rated for each examination and compared between sequences (Fisher exact tests).

Results: Significant differences were identified between DCE-MRI sequences. E_{max} increased significantly at higher FAs and with linear *k*-space sampling ($P < .0001$; $P = .001$). Radial protocols exhibited greater T_{max} than linear protocols at FAs of both 14° ($P = .025$) and 18° ($P < .0001$), suggesting artificially flattened uptake curves. Good correlation was observed between E_{calc} and E_{max} ($r = 0.86$). Fat suppression failure was more pronounced at an FA of 18° ($P = .008$).

Conclusions: This retrospective approach is validated as a tool to compare and optimize breast DCE-MRI sequences. Alterations in FA and *k*-space sampling result in significant differences in CA uptake curve shape which could potentially affect diagnostic interpretation. These results emphasize the need for careful parameter selection and greater standardization of breast DCE-MRI sequences.

Key Words: Breast imaging; MRI; contrast agents; enhancement; quality assurance.

Acad Radiol 2014; 21:1394–1401

From the Cancer Research - United Kingdom (CR-UK) Cancer Imaging Centre, Institute of Cancer Research and Royal Marsden NHS Foundation Trust, Downs Rd, Sutton, Surrey SM2 5PT, United Kingdom (A.E.W.L., M.B., N.M.dS., M.O.L., M.A.S.); Department of Radiology, Royal Marsden Hospital, Sutton, Surrey, United Kingdom (R.J.E.P., E.D.S., T.W., C.R., M.U., S.A., R.M.W.); and Clinical Research and Development, Royal Marsden Hospital, Sutton, Surrey, United Kingdom (K.T.). Received April 17, 2014; accepted June 27, 2014. Funding Sources: We acknowledge the support received for the CR-UK and the Engineering and Physical Sciences Research Council Cancer Imaging Centre in association with the Medical Research Council and Department of Health (England) (grants C1060/A10334, C1090/A16464 and C16412/A6269), National Institute for Health Research (NIHR) funding to the Clinical Research Facility in Imaging and the Biomedical Research Centre, the Technology Strategy Board (M1550J) and an NIHR Transitional Research Fellowship (TRF-2013-06-003) to A.E.W.L. Conflicts of Interest: M.O.L. holds a nonrenumerated directorship of Specialty Scanners, a company developing breast magnetic resonance imaging (MRI) scanners. The Royal Marsden Hospital (RMH) and The Institute of Cancer Research (ICR) hold research agreements with Siemens and Philips, manufacturers of MRI systems. Software for breast MRI analysis has been developed and licensed by ICR, and M.O.L. may receive payments under the ICR Rewards for Inventors Scheme. A.E.W.L. has been employed on a joint grant between the ICR and Specialty Scanners. M.O.L. is an NIHR Senior Investigator. **Address correspondence to:** M.O.L. e-mail: Martin.Leach@icr.ac.uk

http://dx.doi.org/10.1016/j.acra.2014.06.014

In the evaluation of breast tumors, the Breast Imaging Reporting and Data System lexicon classifies both lesion morphology and the pattern of contrast agent (CA) uptake with time (1,2). Dynamic contrast-enhanced (DCE) magnetic resonance imaging (MRI) is used to increase the specificity of breast MRI examinations, through evaluation of the kinetic behavior of CA uptake (3,4). Enhancement curves may demonstrate persistent, plateau, or wash-out behaviors of signal intensity across the dynamic series, where a wash-out of signal intensity is often indicative of malignancy (5). With smaller lesions in which morphology is indeterminate, this evaluation of CA kinetics becomes increasingly important in diagnosis.

Reliable classification of CA uptake curves requires rapid T_1-weighted pulse sequences to be designed to provide image intensity directly proportional to CA concentration over the range of expected T_1 values. Effective fat suppression is also required to facilitate the assessment of small lesions. Accurate evaluation and standardization of sequence performance is particularly important because differences across magnetic

TABLE 1. Summary of MRI Protocols

System	Philips 1.5 T Intera			Philips 1.5 T Achieva	Philips 1.5 T Intera
Group Notation	Rad-10	Rad-14	Rad-18	Lin-14	Lin-18
Sample size	8	10	10	7	10
Flip angle	10°	14°	18°	14°	18°
K-space sampling	Radial	Radial	Radial	Linear	Linear
TR/TE, ms	5.10/2.39	5.10/2.35	3.94/1.81	4.58/2.27	4.10/1.97
Number of echoes per shot	100	100	60	100	100
Slice thickness, mm	2.5	2.5	2.0	2.0	2.0
In-plane resolution, mm	0.63	0.63	1.25	1.25	1.25

MRI, magnetic resonance imaging; TE, echo time; TR, repetition time.

resonance (MR) systems and sequences can significantly affect sensitivity for detecting lesions (6). However, the accuracy of sequence assessment with test objects is limited: spatial variations in the B_1 field can hinder verification of image intensity dependence on T_1 (7) and the flip angle (FA) applied to a test object may not accurately represent clinical examinations. In addition, variability in patient size and shape and differences in patient circulation affect T_1 values after intravenous CA administration. An assessment of the impact of sequence parameter changes on the diagnostic capability of an examination would therefore be invaluable. As the internal mammary artery provides a source of arterial enhancement in the examination field of view, we used it to construct signal intensity versus time curves retrospectively and compared these curves between patients examined with breast DCE-MRI sequences of varying FAs and *k*-space sampling patterns. We simultaneously assessed the effect of these parameters on fat suppression performance. Every sequence evaluated was used in clinical practice and was therefore compliant with current technical breast screening guidelines (8,9). Sequences with different *k*-space sampling coverage pattern and FA were modeled to validate experimental results.

MATERIALS AND METHODS

MRI Protocols

Routine clinical breast examinations were undertaken at 1.5T (Philips Intera and Achieva; Best, Netherlands) at three separate hospital sites in the same institution. DCE-MRI breast examinations were performed with three-dimensional (3D) fat-suppressed spoiled gradient-echo sequences (Philips Thrive). Modifications associated with changes in clinical practice had resulted in five DCE-MRI sequences that were used for comparison, as detailed in Table 1. These sequences differed primarily in FA values (10°, 14°, and 18°) and *k*-space coverage pattern (linear, denoted "Lin" at 14° and 18°, and radial, denoted "Rad" at 10°, 14°, and 18°). In this study, the linear *k*-space sampling pattern was a segmented centric-ordered Cartesian sampling scheme. For the radial sampling pattern, the data acquisition for each shot started at the *k*-space center and progressed toward the higher spatial frequencies in radial trajectories. Each dynamic series consisted of one precontrast and eight postcontrast axial images, each acquired in approximately 1 minute, in agreement with breast screening guidelines (8,9). A standardized procedure was used for administration of a single dose (adjusted by body weight) of DOTAREM (Guerbet; Villepinte, France) at 2 mL/s (MedRad; Warrendale, PA) followed by a saline flush (20 mL, 2 mL/s). CA was administered immediately after completion of the precontrast data set. For each sequence, seven to ten consecutive patient examinations were selected in chronologic order, with the most recent patient in each DCE-MRI protocol selected first. Retrospective analysis of patient examinations was carried out with the approval of the Clinical Audit Committee.

Theoretical Calculation of Relative Enhancement and Fat Suppression Efficiency

In fat-suppressed spoiled gradient-echo pulse sequences, data acquisition is divided into segments, each preceded by a spectrally selective inversion pulse and containing several successively acquired echoes. Because breast DCE-MRI requires high spatial resolution, the pulse sequences tend to use the shortest possible repetition times (TRs) and echo times (TEs) available and a relatively high number of echoes in each segment (approximately 50–100). These sequences can be modeled numerically, using the Bloch equations (10,11). In the context of breast DCE-MRI simulation, results can be generalized to sequences using similar approaches.

Signal intensity for each breast DCE-MRI sequence was calculated as a function of T_1 using the Bloch equations and in-house software (IDL 7.1 ITTVIS; Boulder, CO) considering both those spins unaffected by the inversion pulse (water) and those inverted (fat). $T_2^\star$ decay was considered negligible for the short TE values used, and was disregarded. Differences in FA, TR, and number of echoes per shot were included in the calculation for each sequence. The adiabatic fast passage fat suppression was modeled as a 180° inversion pulse followed by a 90-millisecond inversion time (12). However, the calculation did not differentiate between linear and radial *k*-space patterns, as the echoes associated with the *k*-space center are the first to be acquired in each segment. However in practice, unlike the

linear *k*-space pattern, the radial sampling pattern oversamples the center of the *k*-space throughout the data acquisition. A value of 1200 milliseconds was chosen to represent precontrast blood T_1 (13) with a corresponding value of 100 milliseconds at maximum peak CA concentration, selected after analysis of 10 examinations within a previous quantitative study (14). Accordingly, maximum relative enhancement, E_{calc}, was calculated as the percentage increase of signal intensity $\{[(SI_{max} - SI_{precontrast})/SI_{precontrast}] \times 100\}$ (5) between these T_1 values. The image intensity for suppressed and unsuppressed fat was calculated, assuming 300 milliseconds to be the T_1 of fat (15). The difference in signal intensities at this T_1 value allowed an evaluation of the theoretical optimum fat suppression efficiency that could be achieved by each DCE-MRI sequence.

Analysis of Dynamic Contrast-Enhanced Examinations

For each examination, the right internal mammary artery was located perpendicular to the axial acquisition plane. An axial slice was selected in a standardized position within the central 5-cm region of the volume of interest, at a point where the artery was clearly distinct from the associated vein (Fig 1). The center of this volume was positioned to axially bisect the nipple because the position of the breasts relative to the coil was presumed to be approximately constant across examinations. To exclude partial volume effects, only the central pixel of the vessel was chosen as the region of interest (ROI) in each dynamic frame. Following this manual registration over the dynamic series, the ROI was used to construct a nine-point signal intensity curve as a function of time. The measured maximum relative enhancement, E_{max}, for each examination was derived from this curve. The time to peak enhancement, T_{max}, was defined and measured as the position in the dynamic series corresponding to maximum contrast uptake.

In addition, values of arterial relative enhancement were measured at each dynamic frame for the selected axial slice in each examination. Mean values of relative enhancement were calculated for each patient group to compare the shape of the enhancement curves for each DCE-MRI sequence across the dynamic series.

Evaluation of Fat Suppression

Patients with any mastectomy or implant ($n = 10$) were excluded from this evaluation. The 3D data set at maximum enhancement was reformatted and a slice selected in each of three orientations—bisecting the nipple in oblique axial and sagittal orientations and an oblique coronal slice parallel and as close to the chest wall as possible. Each slice was examined for evidence of fat suppression failure by considering either 1) bright regions of unsuppressed fat or 2) chemical shift artifact (identified by dark pixels at the boundary between breast fat and parenchyma). A consensus of three experienced observers (A.E.W.L., M.B., and M.A.S.) scored each indicator of fat suppression failure separately as fat suppression "successful" or "unsuccessful."

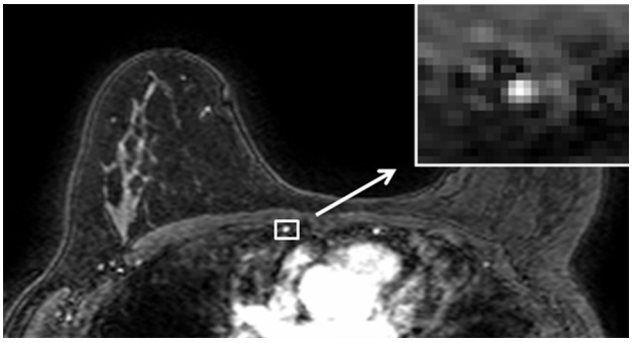

Figure 1. Axial T_1-weighted fat-suppressed dynamic contrast-enhanced magnetic resonance breast image (the first postcontrast dynamic) identifying position of right internal mammary artery together with enlarged image (*inset*). Fat suppression failure in the left breast is also evident.

Data Analysis

Pearson correlation coefficient was used to compare measured values of arterial maximum relative enhancement, E_{max}, with calculated values. Measured values of E_{max} were inspected for normality using box and whisker plots; any outliers identified were not excluded from statistical analyses. Measured values of E_{max} were compared between sequences using two-way analysis of variance, taking FA and *k*-space sampling technique as explanatory variables. Bonferroni post hoc tests were performed to account for multiple testing with a P value $<.05$ indicating significance. Significant variables identified from the analysis of E_{max} were used to construct a stratified analysis of time to peak enhancement, T_{max}. Selected patient groups differing in only one variable were compared using the Mann–Whitney nonparametric test, with a P value $<.05$ taken to be significant.

The binary fat suppression evaluation outcomes for each indication of fat suppression failure were collated for each DCE-MRI sequence. The effect of either *k*-space sampling or FA was compared across the patient cohort for each indication using Fisher exact tests to account for small sample sizes. Because the lack of a 10° FA sequence performed with linear *k*-space sampling was considered to introduce a possible bias, the radial 10° FA group was excluded from this statistical evaluation. Once again, P values $<.05$ were considered to be significant.

RESULTS

Calculation of Relative Enhancement and Fat Suppression Efficiency

Figure 2 plots theoretically calculated unsuppressed signal intensity as a function of $1/T_1$ for T_1 values between the range of 50 milliseconds and 1200 milliseconds for the five DCE-MRI sequences. These covered three FAs of 10°, 14°, and 18°. As expected, sequence differences in TR and number of echoes per shot caused relatively minor variations across

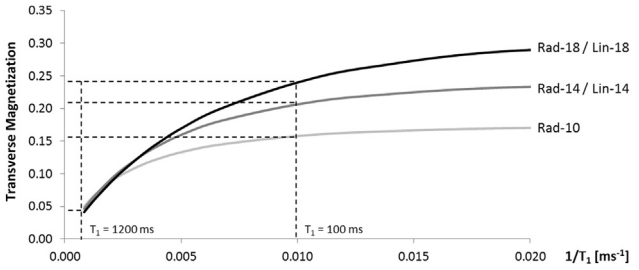

Figure 2. Calculated image intensity (arbitrary units) as a function of $1/T_1$ for the five dynamic contrast-enhanced magnetic resonance imaging sequences (flip angles 10°, 14°, and 18°, respectively). Radial and Linear sequences with the same flip angle appear coincident at this scale. *Hashed lines* represent a T_1 of 1200 milliseconds for unenhanced blood and 100 milliseconds at maximum enhancement. Dynamic range is reduced at lower flip angles.

the rapid high-resolution sequences used. However, because the data associated with the *k*-space center are mapped in the initial part of the segment, FA is the main determinant of contrast and dynamic range. Theoretically, an increase in FA was clearly associated with an increase in dynamic range. Calculated values of maximum relative enhancement, E_{calc}, are displayed in Table 2 and confirm that signal is approximately proportional to FA.

To illustrate dependence of fat suppression on FA, Figure 3 displays both the unsuppressed and suppressed signal intensity (upper black curves and lower gray curves, respectively) as a function of $1/T_1$ for the DCE-MRI sequences, again corresponding to the three FAs of 10°, 14°, and 18°. The relative difference between unsuppressed and suppressed spin signal intensities was greater at lower FAs, indicating that fat suppression efficiency is expected to improve as the FA is reduced.

Analysis of Dynamic Contrast-Enhanced Examinations

Within the chosen slice, the position of the internal mammary artery was observed to drift by as much as 6 mm across the dynamic series. This observation was common across all sequences, and there were no trends in the direction and extent of motion. This movement is likely to arise from a combination of cardiac motion, pulsatility, respiration, and patient movement during the DCE-MRI examination. Even at the lowest resolution, artery diameter was always measured to be in excess of 5 pixels (3–6 mm) with a vessel center ROI of 1 pixel.

Means and corresponding standard deviations of measured E_{max} across the varying sequences are displayed in Table 2. Box plots displaying the population composition for each sequence are displayed in Figure 4 and largely suggested normally distributed data. The calculated coefficient of variation ranged from 0.24 to 0.34 suggesting good intragroup reproducibility. Good correlation was found between measured values of E_{max} and the calculated maximum relative enhancement (r = 0.86). Both FA and *k*-space sampling technique were found to have a statistically significant impact on measured maximum relative enhancement, E_{max} ($P < .0001$ and $P = .001$, respectively). Greater values of E_{max} were found for sequences with an FA of 18° compared to 10° and 14° ($P < .0001$ and $P < .0001$, respectively). Although an FA of 10° exhibited lower E_{max} than 14°, this difference was not found to be statistically significant ($P = .21$). Linear sequences exhibited significantly greater values of E_{max} than radial sequences ($P = .001$).

Figure 5 displays the frame in the dynamic series at which peak enhancement, T_{max}, was observed across the five different DCE-MRI sequences. In particular, the DCE-MRI sequence with an FA of 18° and linear *k*-space sampling consistently recorded T_{max} at the first postcontrast dynamic. However, radial sequences were observed to produce a wider spread in T_{max} and frequently enhanced at later time points than the equivalent linear sequences. Particular pairwise comparisons revealed no statistically significant differences in time to peak enhancement, T_{max}, with changes in FA. However, radial sequences reached peak enhancement at a later time than linear sequences at FAs of both 14° ($P = .025$) and 18° ($P < .0001$).

Figure 6 displays the mean enhancement curves for the sequences with an FA of 14° and 18°. Those curves derived from radial sequences were found to be relatively insensitive to initial CA uptake and possessed reduced amplitude in comparison with their linear counterparts.

Fat Suppression Evaluation

The incidence of bright regions of unsuppressed fat and chemical shift artifact, considered separately in 35 patients, is summarized in Table 3, and the percentage of examinations affected by fat suppression failure is displayed in Figure 7.

Regions of Unsuppressed Fat. There were no significant differences in the failure rate of fat suppression between linear and radial sequences on statistical analysis of the Rad/Lin-14 and Rad/Lin-18 groups ($n = 29$, $P = .264$). Within both radial and linear sequences, the incidence of fat suppression failure was found to increase with FA (Fig 7a); comparison of the Rad/Lin-14 and Rad/Lin-18 groups ($n = 29$) showed this increase to be statistically significant ($P = .008$). These observations agreed with simulations of fat suppression performance (Fig 3), which indicated that fat suppression efficiency would be reduced as the FA increased.

Chemical Shift Artifact. Trends in the incidence of chemical shift artifact did not appear to follow those identified when considering bright regions of unsuppressed fat. Considering the Rad/Lin-14 and Rad/Lin-18 groups, the incidence of chemical shift artifact was not found to differ significantly between radial and linear sequences ($P = .067$). Although Lin-18 exhibited a higher failure rate than Lin-14, any difference in chemical shift artifact with FA was not found to be statistically significant ($P = .274$).

DISCUSSION

Assessment of an arterial input function (AIF) using the internal mammary arteries to compare protocols is a novel approach in breast DCE-MRI. Although location of the

TABLE 2. Values of E_{calc} with Mean and Standard Deviation of Measured E_{max}

System	Philips 1.5 T Intera			Philips 1.5 T Achieva	Philips 1.5 T Intera
Group	Rad-10	Rad-14	Rad-18	Lin-14	Lin-18
E_{calc}, %	220	348	484	367	486
E_{max}, %	113 ± 32	146 ± 35	223 ± 52	196 ± 63	336 ± 112

E_{calc}, calculated maximum relative enhancement; E_{max}, measured maximum relative enhancement.

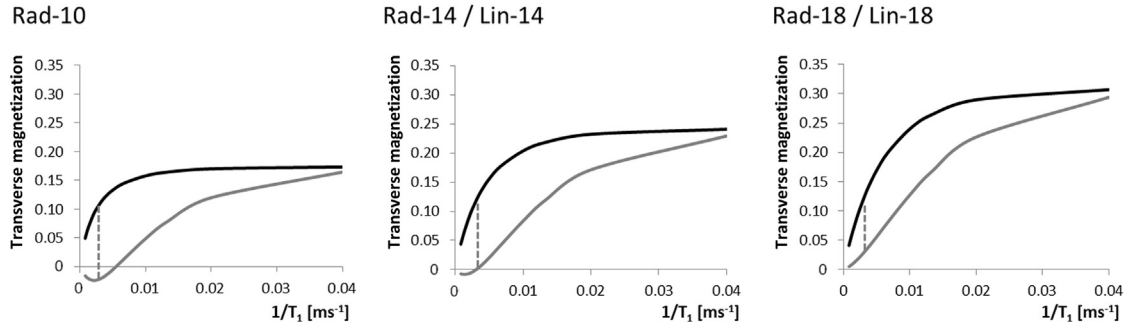

Figure 3. Calculated image intensity (arbitrary units) as a function of $1/T_1$ for the five dynamic contrast-enhanced magnetic resonance imaging sequences (flip angles 10°, 14°, and 18°, respectively). Radial and Linear sequences with the same flip angle appear coincident at this scale. Unsuppressed signal intensity is represented by the *upper black curve*, with the *lower gray curve* corresponding to the suppressed signal intensity. The *hashed line* denotes a T_1 of 300 milliseconds, chosen to represent the T_1 of fat at 1.5 T. At lower flip angles, the relative difference between unsuppressed and suppressed spins is greatest, resulting in the most efficient fat suppression, while dynamic range is reduced.

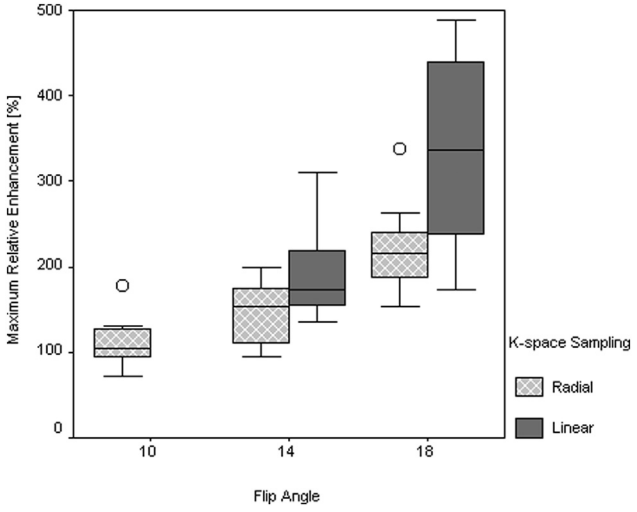

Figure 4. Box plots of E_{max} (maximum relative enhancement) split by flip angle and *k*-space sampling technique. Boxes display median and interquartile range (IQR) and whiskers extend to the extreme values within each group (excluding outliers). Values that fall within IQR 1.5–3 from the outer box limits are defined as outliers and are denoted by an *unfilled circle*.

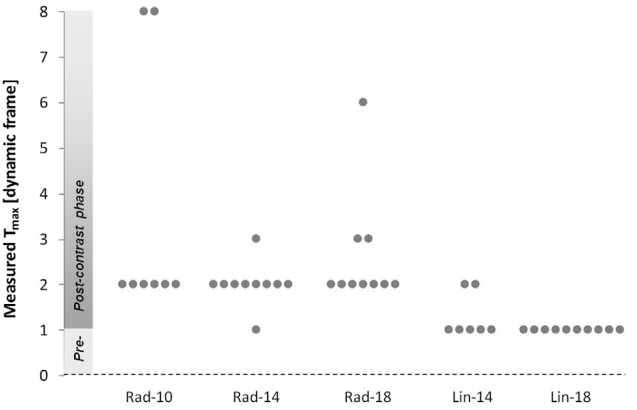

Figure 5. Spread of time to peak enhancement, T_{max} (dynamic frame), across the patient groups. Each dynamic frame was acquired in approximately 1 minute.

internal mammary artery is close enough to the breast coil to yield sufficient signal-to-noise ratio, an ROI within a single vessel is necessarily small. Arterial motion was prevalent across the dynamic series and required registration of the vessel center to adequately minimize the effects of motion. In our data set, cross-sectional vessel area was always sufficient for selection of the brightest pixel, avoiding partial volume effects.

Sequence modeling was performed to validate this new method as a useful investigative quality assurance (QA) tool for breast DCE-MRI sequences. On comparison of E_{max} with E_{calc}, the maximum values of E_{max} within each patient group largely fell short of the calculated value; however, in the Lin-18 group, the maximum E_{max} value was 0.5% greater than that calculated, implying that the shortest blood T_1 value (100 milliseconds) used for peak CA concentration was a reasonable estimate. Physiological differences within a group of patients are likely to have resulted in varying peak CA concentration and CA transit time after administration of a single CA dose. In addition, the *k*-space sampling patterns in both cases contributed toward the observed reduction in E_{max}

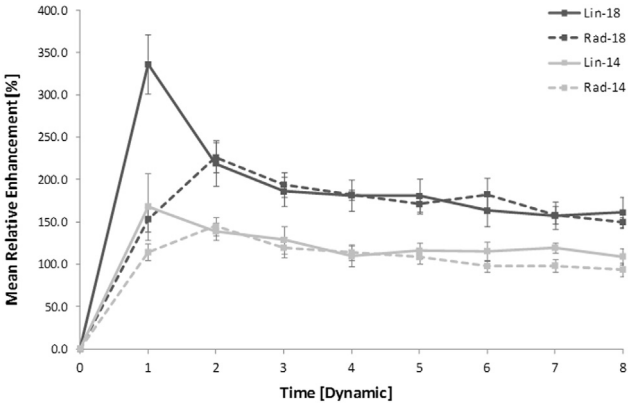

Figure 6. Mean relative enhancement at each dynamic frame in the dynamic series for the dynamic contrast-enhanced magnetic resonance imaging sequences: Lin-18 versus Rad-18 and Lin-14 versus Rad-14. Sequences with the same flip angle but different *k*-space sampling exhibit a reduction in relative enhancement and enhance later in the dynamic series.

against calculated values, albeit for different reasons. In the case of linear *k*-space sampling, the timing of *k*-space center data acquisition was unlikely to coincide with actual peak CA concentration for all patients, and thus, measured E_{max} was expected to be lower than E_{calc} in most cases. For examinations in which data were acquired using the radial *k*-space sampling pattern, oversampling of the *k*-space center throughout data acquisition had an averaging effect which led to a reduction in E_{max}. Nonetheless, the high correlation between E_{calc} and measured E_{max} values supports the methodology used in this study.

The two *k*-space sampling schemes compared in this study resulted in CA enhancement curves with significant differences. Statistical analysis of E_{max} identified that the radial *k*-space sampling pattern led to a lower dynamic range than the linear *k*-space coverage. This reduction in dynamic range was also associated with later and more variable T_{max} suggesting that the radial CA uptake curves were artificially flattened by data averaging. Although the postcontrast curve classification was unaffected, the *k*-space sampling patterns used in this study have been shown to affect characterization of the initial enhancement phase. This result could potentially affect interpretation, particularly as the percentage increase in signal intensity during CA uptake is often used as an important diagnostic and/or prognostic parameter (16). However, there are numerous ways to implement both linear and radial *k*-space sampling schemes across different MR systems and manufacturers. *K*-space sampling schemes should therefore be carefully considered when optimizing DCE-MRI breast protocols and in standardization for multicenter trials.

A reduction in FA was also clearly associated with a reduction in dynamic range and indicated that low FAs might not preserve the approximately linear relationship between image intensity and $1/T_1$ for the range of T1 values expected in breast DCE-MRI examinations. Because the classification of CA uptake curves relies on this linear relationship, a reduction in dynamic range may distort CA uptake curves, potentially affecting curve classification and thus the sensitivity and specificity of breast DCE-MRI.

An evaluation of fat suppression performance in clinical breast examinations is difficult because failure may only affect part of the breast; in this study, the examinations affected by fat suppression failure were still of diagnostic quality. In addition, our evaluation considered only small sample sizes because the Rad-10 group was excluded as well as those patients with mastectomies or implants. The presence of bright regions of unsuppressed fat was unaffected by *k*-space sampling technique but increased at higher FAs, in agreement with computational results. The theoretical influence of FA on fat suppression artifacts was also noted by Desmond et al. (17). Chemical shift artifact was unrelated to either *k*-space or FA and appeared to be more closely linked to the value of TE set for each sequence (Fig 7b): sequences with TE values approaching out of phase values for fat (2.2 milliseconds at 1.5 T), such as Rad-10 and Rad-14, (TE values of 2.40 and 2.35 milliseconds, respectively), exhibited a high incidence of chemical shift artifact. This suggests that TE is an important parameter, often overlooked. Although fat suppression performance can be improved at lower FAs, this unavoidably reduces the dynamic range of an examination. If the wash-in and wash-out phase of an enhancement curve is less distinct, this may result in misclassification of highly perfused tissue with a type I or II curve. At higher FAs, a greater dynamic range is assured, conferring a greater confidence in enhancement curve classification but at the expense of fat suppression efficiency. The need for compromise when selecting FA to optimize dynamic range and fat suppression efficiency (12) is highlighted in our study.

Research has demonstrated the differences in kinetic data that can arise between MR systems (6,18). Breast literature discusses DCE-MRI pulse sequences with special attention given to spatial and temporal resolution (19,20). This study highlights the effect of other parameters, demonstrating significant differences associated with changes in FA and *k*-space coverage which can be easily overlooked: although all the sequences studied complied with the breast DCE-MRI guidelines for temporal resolution (8,9), the variations in parameters selected may have contributed to the variation in reporting and help explain differences in specificity recorded for DCE-MRI (3,21,22).

Although a standardized QA program for breast DCE-MRI can aid assessment and comparison of pulse sequences (8), validation of the relationship between T_1 and image intensity using test objects can be challenging because of B_0 and B_1 inhomogeneity (7). In addition, there are pitfalls in verifying fat suppression with test objects, as they do not reproduce the breast shape and the associated challenge to shimming (23). In contrast, this retrospective analysis of clinical examinations has informed us directly on the significance of a parameter change within the context of the variable circulation patterns in our patient population. The methods outlined in this article are sensitive, require small patient

TABLE 3. Evaluation of Fat Suppression Performance Across the Patient Groups

	Unsuppressed Fat			Chemical Shift Artifact		
Group	Fat Suppression Successful	Fat Suppression Unsuccessful	Total	Fat Suppression Successful	Fat Suppression Unsuccessful	Total
Rad-10	6 (100.0)	0 (0.0)	6	1 (16.7)	5 (83.3)	6
Rad-14	5 (83.3)	1 (16.7)	6	0 (0.0)	6 (100.0)	6
Rad-18	4 (57.1)	3 (42.9)	7	5 (71.4)	2 (28.6)	7
Lin-14	6 (85.7)	1 (14.3)	7	6 (85.7)	1 (14.3)	7
Lin-18	1 (11.1)	8 (88.9)	9	6 (66.7)	3 (33.3)	9
Total			35			35

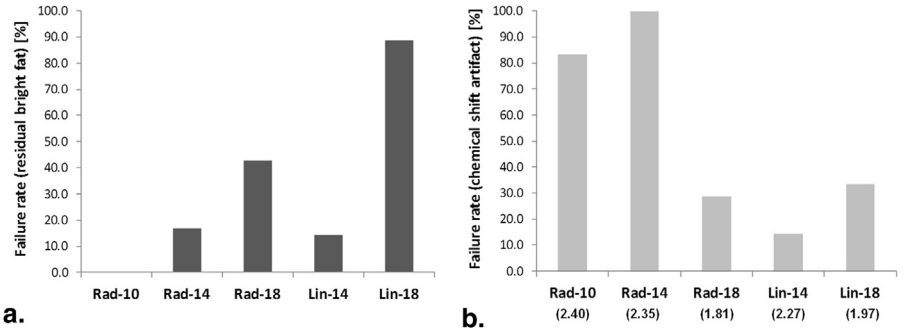

Figure 7. **(a)** Percentage of examinations exhibiting bright regions of unsuppressed fat within each patient group; **(b)** percentage of examinations affected by chemical shift artifact within each patient group, together with set echo time values (milliseconds) for each dynamic contrast-enhanced magnetic resonance imaging sequence.

numbers, and could be adopted as a useful QA tool to ensure system parity.

Our study was subject to some limitations. First, the method we developed to compare the dynamic range in breast DCE-MRI sequences relies on a number of hypotheses: 1) the mammary arteries supplying the breasts experience the highest CA concentration in breast DCE-MRI, 2) the CA concentration within the mammary arteries is independent of breast pathology, and 3) the native T_1 of blood does not vary significantly in the patient population. While underlying physiological differences contribute to the variability observed, the ability to detect statistically significant differences in dynamic range derived from parameter changes in relatively small patient groups would appear to support these hypotheses. Second, the protocols investigated were run on three MRI scanners at our institution, although each scanner was sourced from the same MRI vendor at the same field strength and was regularly subject to identical QA measurements from the same team of clinical scientists. Although data within each protocol group were acquired from the same scanner, we cannot exclude that some changes might be system dependent. In addition, our evaluation analyzed DCE-MRI sequences from a single MRI manufacturer: as mentioned previously, variations in 3D gradient-echo sequence implementation and linear or radial *k*-space coverage options vary with MRI systems and manufacturers. Third, we restricted the analysis of curve shape to several simple, yet quantitative, descriptors of enhancement which reflect clinical practice. Direct comparison of receiver operating characteristic (ROC) curves associated with different pulse sequences requires a prohibitively large number of subjects. Freed considers a different approach using mathematical modeling, and suggests improvement to ROC curves by careful choice of FA and TR (24). The methods developed in this study could contribute toward the theoretical simulation of breast ROC curves by providing a measured AIF together with an assessment of AIF variability within the patient population.

In conclusion, use of the internal mammary artery to estimate an AIF has been demonstrated as a QA method to assess the effect of parameter variations on the shape of the CA uptake curve. We have demonstrated key differences in dynamic range and fat suppression efficiency between guideline-compliant DCE-MRI sequences with varying FA and *k*-space sampling. At our institution, this evaluation resulted in the selection of a 14° FA as the best compromise between dynamic range and fat suppression performance. In addition, the linear *k*-space sampling used in this study is preferred to further increase the dynamic range and optimize the sequence for CA transit time. Sequence specifications for breast DCE-MRI should consider the effect of FA and *k*-space sampling schemes, particularly for studies across multiple systems or institutions.

REFERENCES

1. BI-RADS. MRI Breast Imaging Reporting and Data System. BI-RADS At. Reston, VA: American College of Radiology, 2003.

2. Mahoney MC, Gatsonis C, Hanna L, et al. Positive predictive value of BI-RADS MR imaging. Radiology 2012; 264(1):51–58.
3. Heywang-Köhbrunner S, Bick U, Bradley W, et al. International investigation of breast MRI: results of a multi-centre study (11 sites) concerning diagnostic parameters for contrast-enhanced MRI based on 519 histopathologically correlated lesions. Eur Radiol 2001; 11:531–546.
4. Schnall MD, Blume J, Bluemke DA, et al. Diagnostic architectural and dynamic features at breast MR imaging: multicenter study. Radiology 2006; 238(1):42–53.
5. Kuhl CK, Mielcareck P, Klaschik S, et al. Dynamic breast MR imaging: are signal intensity time course data useful for differential diagnosis of enhancing lesions? Radiology 1999; 211(1):101–110.
6. Jansen SA, Shimauchi A, Zak L, et al. Kinetic curves of malignant lesions are not consistent across MRI systems: need for improved standardization of breast dynamic contrast-enhanced MRI acquisition. Am J Roentgenol 2009; 193(3):832–839.
7. Azlan CA, Ahearn TS, Di Giovanni P, et al. Quantification techniques to minimize the effects of native T1 variation and B1 inhomogeneity in dynamic contrast-enhanced MRI of the breast at 3 T. Magn Reson Med 2012; 67(2):531–540.
8. Clayton D, Davison C, Bailey C, et al. Technical guidelines for magnetic resonance imaging for the surveillance of women at higher risk of developing breast cancer (NHSBSP Publication No 68) p. 1–31.
9. Breast Magnetic Resonance Imaging (MRI) Accreditation Program Requirements. Reston, VA: American College of Radiology, 2012; 1–16.
10. Bloch F. Nuclear induction. Phys Rev 1946; 70(7-8):460–474.
11. Slichter C. Principles of magnetic resonance. In: Cardona M, Fulde P, von Klitzing K, et al., eds. Berlin, Heidelburg, New York: Springer-Verlag, 1980.
12. Schmidt M, Borri M, Scurr E, et al. Breast dynamic contrast-enhanced examinations with fat suppression: are contrast-agent uptake curves affected by magnetic field inhomogeneity? Eur Radiol 2013; 23(6): 1537–1545.
13. Bernstein MA, King KF, Zhou XJ. Handbook of MRI pulse sequences. Philadelphia, PA: Elsevier Academic Press, 2004.
14. Leach MO, Boggis CRM, Dixon AK, et al. Screening with magnetic resonance imaging and mammography of a UK population at high familial risk of breast cancer: a prospective multicentre cohort study (MARIBS). Lancet 2005; 365(9473):1769–1778.
15. Rakow-Penner R, Daniel B, Yu H, et al. Relaxation times of breast tissue at 1.5T and 3T measured using IDEAL. J Magn Reson Imaging 2006; 23(1): 87–91.
16. Turnbull LW. Dynamic contrast-enhanced MRI in the diagnosis and management of breast cancer. NMR Biomed 2009; 22(1):28–39.
17. Desmond KL, Ramsay EA, Plewes DB. Comparison of biphasic and reordered fat suppression for dynamic breast MRI. J Magn Reson Imaging 2007; 25(6):1293–1298.
18. Pabst T, Kenn W, Kaiser WA, et al. Understanding why contrast enhancement in dynamic MRI is not reproducible: illustration with a simple phantom. Breast J 2001; 7(3):166–170.
19. Kuhl C. The current status of breast MR imaging. Part 1: Choice of technique, image interpretation, diagnostic accuracy and transfer to clinical practice. Radiology 2007; 244:356–378.
20. Moon M, Cornfield D, Weinreb J. Dynamic contrast-enhanced breast MR imaging. Magn Reson Imaging Clin N Am 2009; 17:351–362.
21. Heywang-Köbrunner SH, Viehweg P, Heinig A, et al. Contrast-enhanced MRI of the breast: accuracy, value, controversies, solutions. Eur J Radiol 1997; 24:94–108.
22. Berg W, Gutierrez L, NessAiver M, et al. Diagnostic accuracy of mammography, clinical examination, US and MR imaging in preoperative assessment of breast cancer. Radiology 2004; 233:830–849.
23. Maril N, Collins CM, Greenman RL, et al. Strategies for shimming the breast. Magn Reson Med 2005; 54(5):1139–1145.
24. Freed M. Effect of protocol parameters on contrast agent washout curve separability in breast dynamic contrast enhanced MRI: a simulation study. Magn Reson Med 2012; 68:516–522.